SANDIA REPORT
SAND2007-7679
Unlimited Release
Printed Month and Year

Novel Photonic Crystal Cavities and Related Structures

Ting S. Luk

Prepared by
Sandia National Laboratories
Albuquerque, New Mexico 87185 and Livermore, California 94550

Sandia is a multiprogram laboratory operated by Sandia Corporation,
a Lockheed Martin Company, for the United States Department of Energy's
National Nuclear Security Administration under Contract DE-AC04-94AL85000.

Issued by Sandia National Laboratories, operated for the United States Department of Energy by Sandia Corporation.

Available to DOE and DOE contractors from
U.S. Department of Energy
Office of Scientific and Technical Information
P.O. Box 62
Oak Ridge, TN 37831

Telephone: (865) 576-8401
Facsimile: (865) 576-5728
E-Mail: reports@adonis.osti.gov
Online ordering: http://www.osti.gov/bridge

Available to the public from
U.S. Department of Commerce
National Technical Information Service
5285 Port Royal Rd.
Springfield, VA 22161

Telephone: (800) 553-6847
Facsimile: (703) 605-6900
E-Mail: orders@ntis.fedworld.gov
Online order: http://www.ntis.gov/help/ordermethods.asp?loc=7-4-0#online

SAND2007-7679
Unlimited Release
Printed Month Year

Novel Photonic Crystal Cavities and Related Structures

Ting S. Luk
Photonic Microsystems Technology
Sandia National Laboratories
P.O. Box 5800
Albuquerque, New Mexico 87185-MS1080

Abstract

The key accomplishment of this project is to achieve a much more in-depth understanding of the thermal emission physics of metallic photonic crystal through theoretical modeling and experimental measurements. An improved transfer matrix technique was developed to enable incorporation of complex dielectric function. Together with microscopic theory describing emitter radiative and non-radiative relaxation dynamics, a non-equilibrium thermal emission model is developed. Finally, experimental methodology was developed to measure absolute emissivity of photonic crystal at high temperatures with accuracy of +/-2%. Accurate emissivity measurements allow us to validate the procedure to treat the effect of the photonic crystal substrate.

ACKNOWLEDGMENTS

The successful completion of this project is the result of the efforts of many people. Weng Chow and Ihab developed the microscopic theory of thermal emission. Tim McLellan did much of the data acquisition of the thermal emission experiment. Ganesh Subramania helped to ensure the sample is properly released. Finally, Robert Ellis provided many helpful suggestions.

Table of content

Introduction

A three dimensional photonic crystal is inherently an optical cavity allowing photonic confinement all three dimensions. Photonic crystal is fundamentally different optical device which has functionalities beyond optical filters and optical waveguides. It is a 3D optical cavity which has entirely different photonic density-of-states entirely different from the free-space. Modification of free-space density-of-states in photonic crystal is because of its periodic property in the dielectric constant. As a result its thermal emission properties can be quite different and stimulate us to revisit the fundamental nature of the Planck radiation law.

The Planck blackbody distribution formula assumes infinitely fast relaxation dynamics so that the emitter population is always described by the Maxwell-Boltzmann distribution. Several factors could cause deviation from equilibrium, including compression of free-space photon density of states by a photonic crystal, and spectral hole burning arising from disparities among excitation, emission and relaxation rates. The thermal emission model here uses a fully-quantized active photonic crystal theory to incorporate a detailed description of relaxation processes will be presented. Nonequilibrium effects, e.g., electronic population heating and spectral hole burning, will be described within the context of an effective relaxation rate treatment. This is the only theoretical model that can address non-equilibrium dynamics of photonic crystal emissions. In addition, careful and accurate experimental measurements are made on the thermal emission of tungsten photonic crystal. We have developed a methodology to compare emission measurement in the presence of substrate with theoretical calculations of reflectance and transmission without the substrate.

Another aspect of this type of novel cavity is its interaction with free-space. In reality, a photonic crystal is not infinite in extent and is typically coupled to the free-space on one side of the crystal and a silicon substrate on the other side.

Theoretical treatment using transfer matrix method (TMM) has been developed under this project is capable to include defect cavity in 3D photonic crystal. In addition, this model is capable of handling lossy dielectric material, i.e. complex dielectric constant.

In this report, we describe in detail the thermal emission model, absolute emissivity measurement and transfer matrix computational method developed.

1. Emission from an active photonic crystal

We investigated theoretically the emission from an active photonic crystal. Redistribution of photon density of states by a photonic lattice was found to greatly influence the thermal emission spectrum, resulting in substantial deviation from the Planck distribution. The calculation predicts that the photonic lattice intensity may exceed that of a blackbody source within certain spectral regions. However, the excess emission may be lost in practice because of nonradiative losses and photonic lattice inhomogeneities.

1.1 Introduction

In the presence of a photonic crystal host, a multitude of novel optical phenomena arise because of two main features of a photonic lattice band structure: suppression of photon density of states along certain crystallographic directions and propagation of selected Bloch-modes as mandated by translational symmetry. Examples of novel phenomena include, inhibition of spontaneous emission[1,2], reduced group velocity [3], exceedingly high cavity-*Q* factors [4], low threshold lasing [5], and modified emission characteristics [6,7]. This paper focuses on the last phenomenon, where it was shown that a dielectric photonic crystal can funnel thermal radiation into narrow radiation bands [7]. While there are theoretical and experimental results indicating exceedingly high intensities at the photonic lattice band edge, the question of whether these intensities exceed those of a blackbody at the same temperature and wavelength is unresolved [6,8,9]. An answer is important for scientific understanding and engineering development of a new generation of optical sources and detectors whose properties may go beyond the standard quantum limits. A problem with arriving at an answer experimentally is the difficulty in ensuring that the comparison is made under the same conditions.

The aim of this study is to address the question of thermal radiation from photonic lattices theoretically. Our approach begins with a first-principles calculation of the photonic lattice band structure. The results are used in a model of an active photonic crystal consisting of an inhomogeneously broadened ensemble of two-level systems interacting with a quantized multimode radiation field, whose modal properties are determined by the photonic lattice band structure [10]. The composite system is excited by an external pump and allowed to equilibrate with a thermal bath via collisions. Section II describes the theoretical model, where approximations are made to facilitate the comparison of photonic crystal and blackbody emissions. Results are presented in Sec. III for the limiting cases determined by experimental conditions. To evaluate the model, we show that it retrieves Planck's blackbody distribution in the absence of a photonic crystal, and that the emission peak wavelengths and relative intensities are consistent with experimental values obtained for a lattice subjected to similar conditions.

1.2 Theory

In formulating the problem, we label each two-level system with n, so that $|a_n\rangle$ and $|b_n\rangle$ are the ground and excited states, respectively, that are separated by energy ωn. Correspondingly, each radiation field mode as energy Ω_k, and is described by creation and annihilation operators $a_k^\dagger$ and a_k, respectively. The relation between Ω_k and k depends on the

photonic lattice structure. The Hamiltonian for the combined matter and radiation field system is [10,11]

$$H = \sum_n \hbar\omega_n |b_n\rangle\langle b_n| + \sum_k \hbar\Omega_k a_k^+ a_k - \sum_{k,n} g_k \left(|b_n\rangle\langle a_n| a_k + a_k^+ |a_n\rangle\langle b_n| \right) \quad (1)$$

where the dipole interaction is assumed, with

$$g_k = \mu \sqrt{\frac{\hbar\Omega_k}{\varepsilon_0 V}}, \quad (2)$$

μ is the dipole matrix element, ε_0 is the permittivity in vacuum, and V is the system volume. Introducing the operators for the microscopic polarization amplitude $\sigma_n{}^+ A_n \equiv |b_n\rangle\langle a_k| \exp[-i(\omega_n - \Omega_k)t]$, the excited and ground state populations, $\sigma_{an} \equiv |a_n\rangle\langle a_n|$ and $\sigma_{bn} \equiv |b_n\rangle\langle b_n|$, respectively, and working in the Heisenberg picture, we derive

$$\frac{d\sigma_n^+ A_k}{dt} = \frac{i}{\hbar} \sum_{k'} g_{k'} \left(\sigma_{bn} A_k A_{k'}^+ - A_{k'}^+ A_k \sigma_{an} \right) e^{-i\left(\omega_n - \Omega_{k'}\right)t}, \quad (3)$$

$$\frac{d\sigma_{an}}{dt} = \frac{i}{\hbar} \sum_k g_k \left(A_k^+ \sigma_n e^{-i(\omega_n - \Omega_k)t} - \sigma_n^+ A_k e^{i(\omega_n - \Omega_k)t} \right), \quad (4)$$

$$\frac{d\sigma_{bn}}{dt} = -\frac{i}{\hbar} \sum_k g_k \left(A_k^+ \sigma_n e^{-i(\omega_n - \Omega_k)t} - \sigma_n^+ A_k e^{i(\omega_n - \Omega_k)t} \right), \quad (5)$$

Additionally, the photon number operator obeys,

$$\frac{dA_k^+ A_k}{dt} = \frac{i}{\hbar} \sum_n g_k \left(A_k^+ \sigma_n e^{-i(\omega_n - \Omega_k)t} - \sigma_n^+ A_k e^{i(\omega_n - \Omega_k)t} \right), \quad (6)$$

Assuming that the polarization dephasing rate γ is much faster than the time variations in the active medium and photon populations, one may adiabatically eliminate the polarization equation. Then, introducing the expectation values $n(\Omega,t) = \langle A^+_k(t)\, A_k(t)\rangle$, $n_a(\omega_n,t) = \langle \sigma_{an}(t)\rangle$ and $n_b(\omega_n,t) = \langle \sigma_{bn}(t)\rangle$, we obtain the working equations for our analysis,

$$\begin{aligned} \frac{dn_a(\omega_n,t)}{dt} = {} & \frac{2\pi}{\hbar^2} \rho(\omega_n) g(\omega_n)^2 \left[\{ n_b(\omega_n,t) - n_a(\omega_n,t) \} n(\omega_n,t) + n_b(\omega_n) \right] \\ & - \gamma_n(\omega_n) \{ n_a(\omega_n,t) - f_a(\omega_n,T) \} - \Lambda(\omega_n) n_a(\omega_n,t), \end{aligned} \quad (7)$$

$$\frac{dn_b(\omega_n,t)}{dt} = -\frac{2\pi}{\hbar^2}\rho(\omega_n)g(\omega_n)^2\left[\{n_b(\omega_n,t)-n_a(\omega_n,t)\}n(\omega_n,t)+n_b(\omega_n)\right] \\ -\gamma_n(\omega_n)\{n_b(\omega_n,t)-f_b(\omega_n,T)\}-\Lambda(\omega_n)n_a(\omega_n,t), \tag{8}$$

$$\frac{dn(\Omega,t)}{dt} = \frac{2}{\hbar^2}g^2(\Omega)\sum_n \frac{\gamma}{(\omega_n-\Omega)^2+\gamma^2}\left[\{n_b(\omega_n,t)-n_a(\omega_n,t)\}n(\Omega,t)+n_b(\omega_n,t)\right] \\ -\gamma_c n(\Omega,t), \tag{9}$$

where (Ω) is the photonic-lattice density of states, which is assumed to be spherically symmetric. Additionally, the pump and decay contributions are included phenomenologically, where $_c$ is the photon decay rate,

$$\Lambda(\omega_n) = \Lambda_0 \exp\left(-\frac{\hbar\omega_n}{k_B T_p}\right) \tag{10}$$

is the pump rate, and $_r$ is the effective rate for the actual populations n_a and n_b to relax to the equilibrium distributions

$$f_a(\omega_n,T) = Z_0, \tag{11}$$

$$f_b(\omega_n,T) = Z_0 \exp\left(-\frac{\hbar\omega_n}{k_B T}\right) \tag{12}$$

where Z_o is the thermodynamic partition function that is determined by the total number of two-level systems $N_o = {}_n[f_a(\omega_n)+ f_b(\omega_n)]$, T_p and T are the pump and reservoir temperatures. Solving Eqs. (7)–(9) gives the photon population inside the photonic lattice.

To relate to experiments, it is necessary to obtain the emission outside the photonic lattice. Theoretically, this is a nontrivial step because in our attempt to properly treat the active medium and its emission physics with a quantum theory, we relied on orthonormal optical modes for an infinite photonic lattice. This is very similar to a long-standing problem in laser theory [12]. There, one circumvents the issue by beginning with the Fox-Li modes for a Fabry-Perot cavity with perfectly reflecting mirrors, and then introducing a loss mechanism to represent the outcoupling [13, 14, 15]. Following this approach, we use the steady state solutions $n(\Omega, t)$ $n(\Omega)$ in

$$u(\lambda) = \Gamma(\lambda)\frac{d\Omega}{d\lambda}\hbar\Omega\rho(\Omega)n(\Omega) \tag{13}$$

to obtain the emission wavelength spectrum outside the photonic lattice enclosure, where

$$\Gamma(\lambda) = 1-\left[R(\lambda)+A(\lambda)\right] \tag{14}$$

is the coupling factor describing the efficiency with which radiation inside the photonic crystal is coupled to the outside, $R(\lambda)$ is the reflectivity, $A(\lambda)$ is the absorption. The determinationof $R(\lambda)$ and $A(\lambda)$ is described in the following section.

1.3 Results

In this study, we consider a tungsten Lincoln-log photonic crystal with 28.5% filling fraction and square cross-section rods. A coupled-wave method is used to compute the band structure, where the fields and dielectric functions are expanded in terms of plane waves. Maxwell's equations are cast in an eigen problem format in Fourier space and solved using a transfer matrix approach by treating each layer of the structure as an independent 2D Lamellar grating. Details of this method and its accuracy in describing our structure are discussed elsewhere [16]. The reflectivity $R(\lambda)$ and absorption $A(\lambda)$ are obtained by an independent frequency domain transfer matrix calculation performed on six layers of the photonic crystal structure [17]. Figure 1(a) shows the photonic-lattice dispersion in the (001) crystallographic direction (solid curve). Clearly visible are the fundamental and first higher order gaps, as well as the significant flattening of the dispersion at the band edges due to anticrossing. The dots in Fig. 1(b) give the density of states (DOS) (ω) computed from the dispersion, assuming spherical symmetry. Note the drastic increases in DOS as the photonic crystal dispersion flattens at the band edges. For comparison, Fig. 1 also shows the free-space dispersion and DOS (dashed curves).

Using the photonic-crystal DOS in Fig. 1(b), Eqs. (7)–(9) are solved numerically with a fourth-order Runge-Kutta finite difference method. Following previous comparisons of photonic crystal and blackbody emissions, we ensure that the steady-steady active-medium populations $n_a(\omega_n)$ and $n_b(\omega_n)$ are to a good approximation given by the equilibrium distributions $f_a(\omega_n, T)$ and $f_a(\omega_n, T)$ by performing the calculations for low excitation and rapid relaxation conditions, specifically, with $= 10^{14}$ s ^{1}, $_r = 10^{12}$ s ^{1}, and $_c = \Lambda_0 = 10^{9}$ s ^{1}. Furthermore, we choose $\mu = e \times 0.5$ nm, $V = 10^{18}$ m ^{3}, $N_0 = 200$ and $T_p = T$. The steady-state solutions to Eqs. (7)–(9), are used in Eq. (13), with two limits (as discussed in the next two paragraphs) to the transmission function, to obtain the emission spectrum. For the

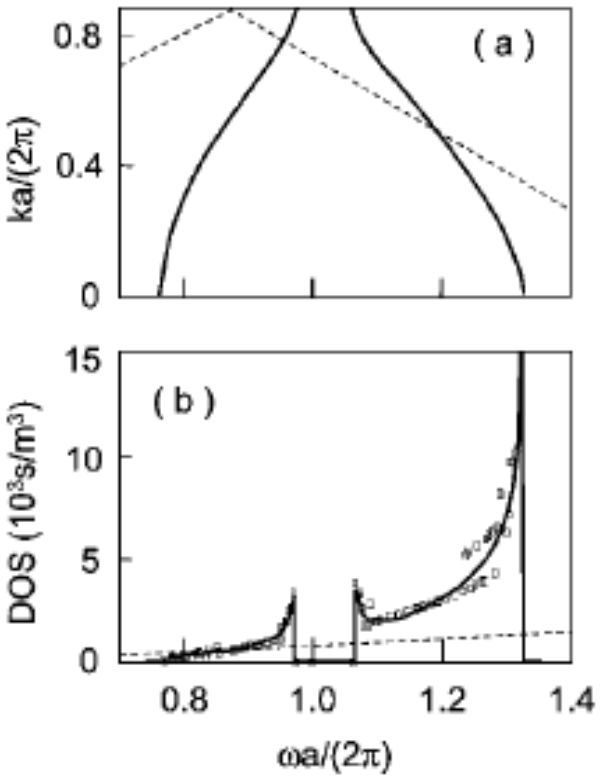

FIG. 1. (a) Calculated photonic-crystal (solid curve) and freespace (dashed curve) dispersions. (b) Densities of states computed from the photonic-crystal _dots_ and free-space (dashed curves) dispersions in (a). The solid line is the least-squares fit to the dots.

corresponding blackbody emission, we repeat the procedure with (ω) replaced by the freespace DOS and with Γ(λ)=1.

The coupling factor depends on experimentally imposed boundary conditions. To estimate the upper emission limit, we consider the best-case scenario of negligible nonradiative losses, so that every photon absorbed by the photonic lattice structure is eventually remitted into a propagating Blochmode. We approximate this situation with a maximum coupling factor of $\Gamma_{max}(\lambda) = 1$ $R(\lambda)$. The solid curves in Fig. 2 show the calculated photonic-crystal emission spectra for this optimal situation at different temperatures. Also plotted are the corresponding blackbody spectra (dashed curves). The figure clearly shows the suppression of photonic lattice emission intensity at the photonic band gaps. More importantly, they indicate a significant increase in intensity at the band edges.

Figure 2 also depicts (with a different vertical scale) the experimentally measured spectra (dotted-dashed curves) for a 6 layer tungsten Lincoln-log structure suspended in vacuum by wires. Nonradiative losses are minimized by having an essentially free-standing structure. The experimental structure was electrically excited by Joule heating. To determine the temperature, the experiment was repeated with blackbody paint coating the central region of the crystal, which then acted as the heating element. Since the blackbody paint behaved essentially as a perfect electrical insulator, it did not change the electrical conductivity of the sample. The temperature was deduced by matching the change in electrical resistivity of the photonic crystal in the two experiments, and using Wein's law for the relationship between temperature and blackbody emission peak. The solid and dotteddashed curves show relatively good agreement between calculation and experiment in terms of the wavelength and relative magnitude of the intensity peaks. Inhomogeneous broadening is included in the

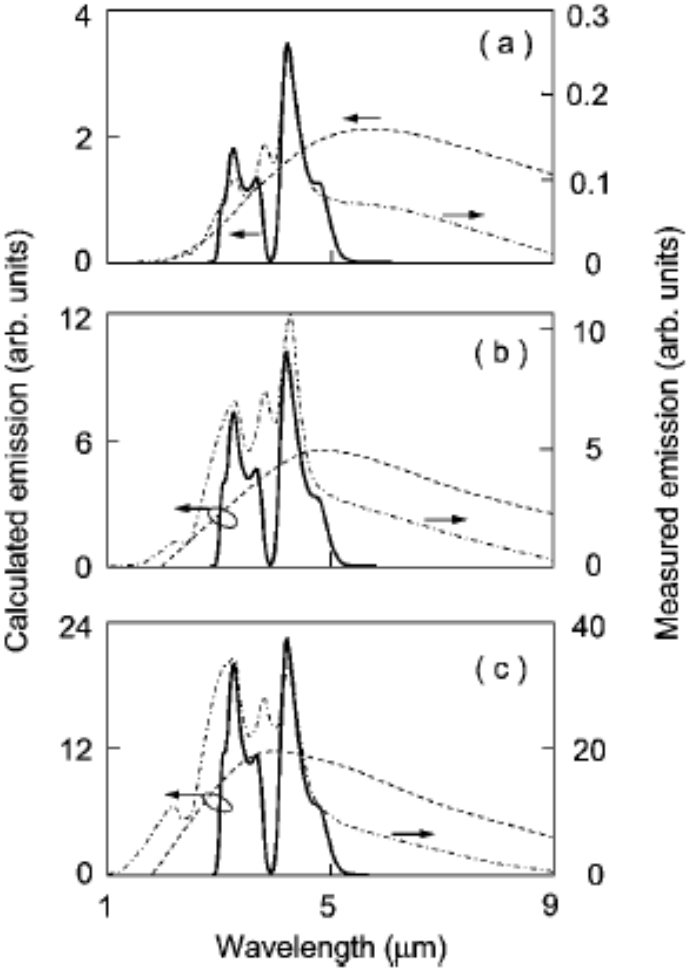

FIG. 2. Calculated blackbody (dashed curve) and lossless photonic-crystal (solid curve) emission spectra for *T*=(a) 500 K, (b) 600 K, and (c) 700 K. The dotted-dashed curves are the experimental spectra.

calculation to account for crystal imperfections. A 5 meV broadening is chosen to match the linewidths of the experimental spectra. Comparison of absolute intensity is not possible because of experimental calibration difficulties. The experimental emission peak at ~2 μm is absent in the calculated results because the bandstructure calculation was terminated at the edge of the second band at ~3 μm.

To obtain a lower bound for the photonic-crystal emission, we consider the worst-case scenario where all the photons absorbed by the photonic lattice structure is lost nonradiatively. To approximate this situation, we use a minimum coupling function of $\Gamma_{min}(\lambda)=1 \quad R(\lambda) \quad A(\lambda)$, where $A(\lambda)$ is calculated using the complex dielectric constant for tungsten [18]. The solid curves in Fig. 3 for the calculated emission spectra at different temperatures, show that for the most part, photonic-crystal emission is at or slightly below the blackbody emission (dashed curves). Comparison with the solid curves in Fig. 2 reveals noticeable spectral shape differences, that are also observed in experiments (compared dotted-dashed curves in Figs. 2 and 3). For the lossy case, the measurements were made with a photonic crystal that is similar to the one used in Fig. 2, but mounted on a heat sink which serves as a channel for nonradiative losses. An inhomogeneous broadening of 20 meV is used in the calculation to match the experimental linewidths. The general agreement between theory and experiment provides some assurance of the accuracy of the transmission coupling functions used in the study.

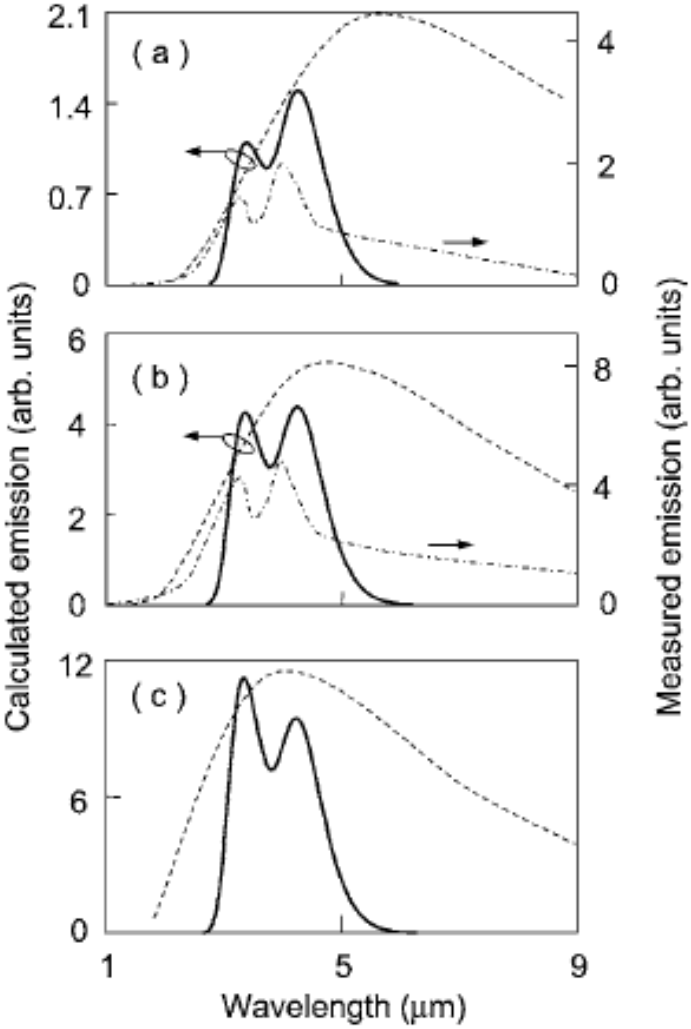

FIG. 3. Calculated blackbody (dashed curve) and lossy photonic-crystal (solid curve) emission spectra for *T*=(a) 500 K, (b) 600 K, and (c) 700 K. The dotted-dashed curves are the experimental spectra.

Figures 4(a) and 4(b) are plots of the ratio between photonic-lattice and blackbody emission for the lossless and lossy cases. In both cases, the curves (displaced vertically for clarity) show the independence of the ratio on temperature, indicating that modifications to the emission by the photon lattice under low excitation and rapid equilibration conditions arise mainly from changes in the photon density of states. Therefore, it is unnecessary to excite an active photon-crystal structure to an extreme temperature to see the predicted effects.

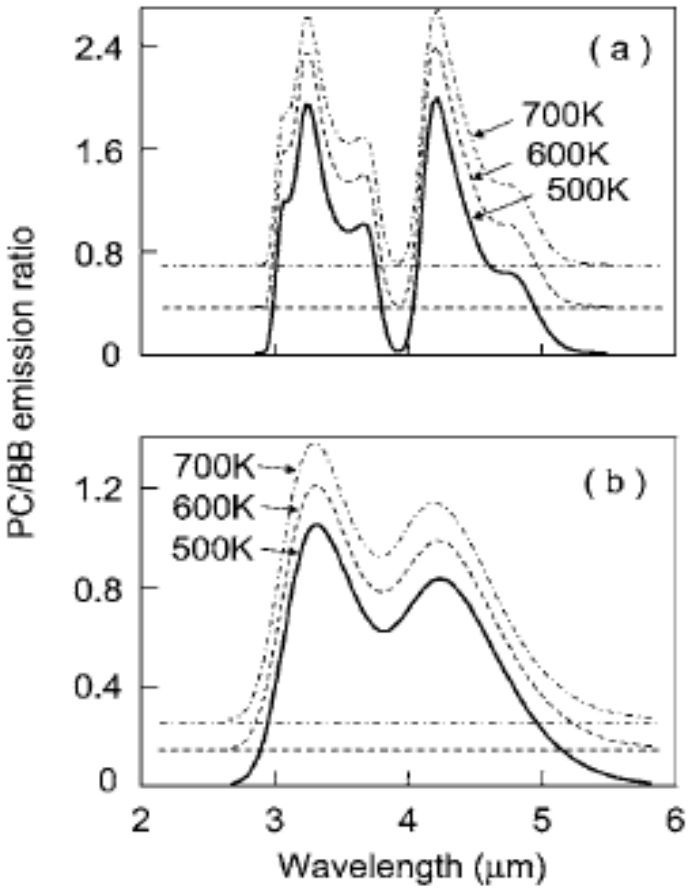

FIG. 4. Ratio of photonic crystal emission to blackbody emission for (a) lossless and (b) lossy cases at different temperatures.

Lastly, we note that inhomogeneous broadening plays an important role in determining the shape and amplitude of the photonic-crystal spectrum. This is the case because of the sharpness of the emission peaks in both lossless and lossy structures. Figure 5 illustrates the dependence of the lossy photonic-crystal spectrum on inhomogeneous broadening. Figures 5(a) and 5(b) show that greater than one photoniccrystal to blackbody intensity ratio is possible even in the lossy structure for inhomogeneously broadening of up to 10 meV. However, when both absorption losses and structural aperiodicities are present the photonic-crystal emission peaks are likely to no longer exceed the blackbody emission, as shown in Fig. 5(c).

1.4 Conclusion

In summary, the emission from an active photonic-lattice crystal is investigated using a model consisting of an inhomogeneously broadened ensemble of two-level systems interacting with a quantized radiation field whose modal properties are determined by the photonic-lattice band structure.

The model gives the emission spectra for arbitrary photoniclattice configurations, and reproduces Planck's radiation formula for thermal emission into free space. Comparison of photonic-lattice and blackbody emission shows appreciable modification of the blackbody spectrum by the photonic lattice, where the redistribution of the photonic density of states results in suppression of emission at certain wavelengths and enhancement at others. Under low excitation and rapid relaxation conditions, the enhancement can give rise to exceedingly

high emission peaks at the photonic lattice band edges, with peak intensities exceeding those of a blackbody at the same temperature and wavelength. However, imperfections, such as those resulting in inhomogeneous broadening, absorption and diffraction losses, can negate the excess emission. Our comparison is between an isolated active photonic crystal system and an isolated blackbody system. The results do not apply to situations involving the coupling of the two systems [9]. There, the interaction between the photonic crystal and blackbody (e.g., leading to population distribution changes) should be taken into account. Finally, the parameter space explored excludes situations involving nonequilibrium population effects, even though these effects can be treated within the framework of the present model.

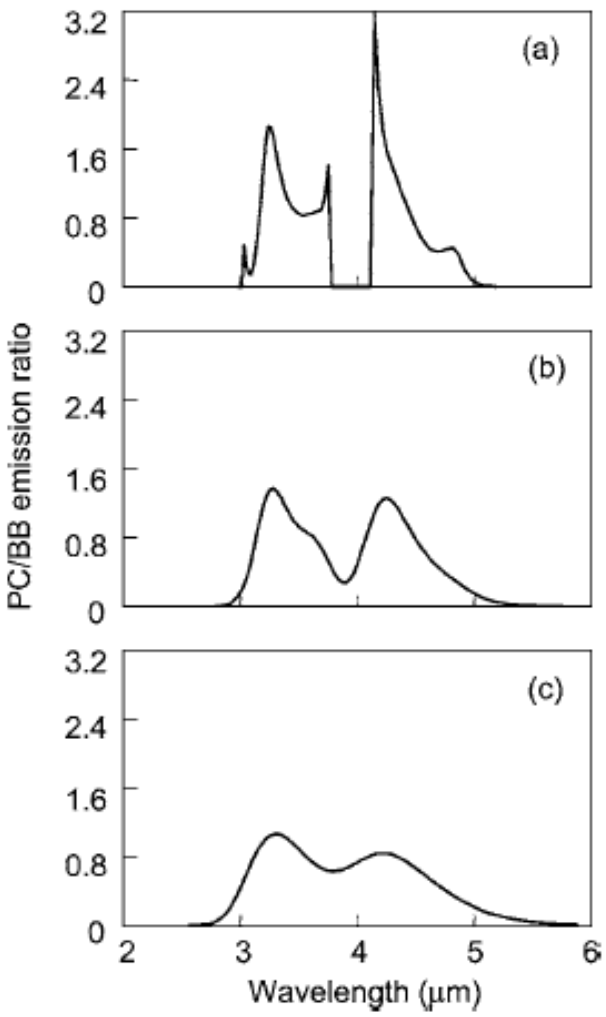

FIG. 5. Ratio of photonic crystal emission to blackbody emission for the lossy case and inhomogeneously broadening of (a) 0, (b) 10, and (c) 20 meV.

1.5 References

[1] E. Yablonovitch, Phys. Rev. Lett. **58**, 2059 (1987).
[2] S. John and J. Wang, Phys. Rev. Lett. **64**, 2418 (1990).
[3] S. John and J. Wang, Phys. Rev. B **43**, 12772 (1991).
[4] G. Subramania, S. Y. Lin, J. R. Wendt, and J. M. Rivera, Appl. Phys. Lett. **83**, 4491 (2003).
[5] O. Painter, R. K. Lee, A. Scherer, A. Yariv, J. D. O'Brien, P. D. Dapkus, and I. Kim, Science **284**, 1819 (1999).
[6] C. M. Cornelius and J. P. Dowling, Phys. Rev. A **59**, 4736 (1999).
[7] S. Y. Lin, J. G. Fleming, E. Chow, J. Bur, K. K. Choi, and A. Goldberg, Phys. Rev. B **62**, R2243 (2000).
[8] J. G. Fleming, S. Y. Lin, and I. El-Kady, Appl. Phys. Lett. **83**, 593 (2003).
[9] T. Trupke, P. Würfel, and M. A. Green, Appl. Phys. Lett. **84**, 1997 (2004).
[10] N. Vats, S. John, and K. Busch, Phys. Rev. A **65**, 043808 (2002).
[12] M. O. Scully and M. S. Zubairy, *Quantum Optics* (Cambridge University Press, Cambridge, 1977).
[13] For a textbook discussion see A. E. Siegman, *Lasers* (University Science Books, Mill Valley, 1986), Chap. 24.
[14] W. E. Lamb, Jr., Phys. Rev. **134**, A1429 (1964).
[15] M. Sargent, III, M. O. Scully, and W. E. Lamb, Jr., *Laser Physics*, (Addison-Wesley, Reading, 1974).
[16] L-L. Lin, Z.-Y. Li, and K.-M. Ho, J. Appl. Phys. **94**, 811 (2003).
[17] Z.-Y. Li and K.-M. Ho, Phys. Rev. B **67**, 165104 (2003).
[18] D. R. Lide, *Handbook of Chemistry and Physics*, 83rd ed. (CRC Press, Boca Raton, 2003).

2. Emissivity measurements of 3D photonic crystals at high temperatures

2.1 Introduction

The emittance of photonic crystals [1] has been a subject of intense study because of the potential use of photonic crystals as high temperature emitters for thermophotovoltaic applications [2, 3, 4]. This potential is due to the fact that photonic crystals are artificial materials with densities of states and spectral shapes that can be engineered. For an non-opaque objects, the "*extended*" Kirchhoff's law must be used to obtain the emissivity, *e*, such that $e = 1\text{-}R(\lambda)\text{-}T(\lambda)$, with $R(\lambda)$ and $T(\lambda)$ being the total reflectivity and transmissivity of the material, respectively. Theoretical predictions based on this approach are called indirect methods [5, 6]. In essence this approach calculates the effective absorptivity of the material that makes up the photonic crystal, convoluting it with the slow light effect of the photonic crystal, itself. This approach does not include the interplay between radiative and non-radiative relaxations of the emitters interacting with the electromagnetic fields inside the photonic crystal field. Alternatively, direct approaches based on quantum optics [7, 8], or stochastic Langevin electrodynamics [9, 10], do not assume an *a priori* maximum of 1 for the emissivity. None of these theoretical approaches consider the fact that photonic crystal often is built on a substrate and has finite number of periods. Therefore, theoretical transmittance and reflectance calculations are often for free-standing photonic crystals of infinite extent. Finally, the question remains whether the thermal excitation of a photonic crystal, with a strongly modified density of states, can be driven out of equilibrium; thus raising the possibility that the emissivity in a certain spectral range can exceed unity [3, 8, 7, 11, 12, 13, 14, 15].

Previous measurements performed on a tungsten photonic crystal in the temperature range of 404-546K [15] have shown that the emissivity is independent of temperature, and can be described *approximately* by $1\text{-}R(\lambda)$. The remaining small discrepancy was attributed to the use of specular reflectance for the $1\text{-}R(\lambda)$ calculation rather than, more correctly, the total reflectance. In these measurements, the transmittance of the photonic crystal-substrate system has not been properly accounted for because of the difficulty in measuring effective transmittance. In addition, the transmittance of the silicon substrate can change significantly with temperature along with resistivity, especially in the temperature range being investigated. Since silicon is a semi-transparent material, the emissivity of the heater block can also affect the measured emissivity. As such, in these experiments the measured emissivity was that of a conglomeration of emitters constituting the heater block, the substrate and the PC lattice. At the end the question remains: how does the reflectance of the photonic crystal-substrate system relate to the inherent reflectivity of a free-standing photonic crystal?

In this paper we report on our high-temperature photonic crystal emissivity measurements, and derive the expression for the emissivity of a photonic crystal-substrate system in terms of the separate photonic crystal and substrate emissivities, and the photonic crystal reflectance based on an "*extended*" Kirchhoff's law. The detailed measurement methodology, and a comparison with a theoretical calculation, is presented.

2.2 Emissivity of combined photonic crystal-substrate system

A photonic crystal supported by a substrate allows for convenient handling of the photonic crystal. However, the substrate effect is often not considered in theoretical calculations of the reflectivity and transmissivity. In this case, a tungsten photonic crystal is built on top of a partially-transparent silicon substrate with an unpolished backside. The light scattering effect from the backside of the substrate, and the partial transparency of the substrate itself, introduce tremendous complications in modeling the transmission and reflection of the system [16, 17]. For a uniform semi-transparent material, the emissivity is expressed in terms of reflectivity and transmissivity [17]. In principle one can obtain the emissivity by measuring the reflectivity and transmissivity of the object; this is called an indirect measure (not to be confused with indirect method in the theoretical approaches). To measure the total reflectance and transmittance of a highly scattered object, an integrating sphere is needed [18]. If the sample also needs to be in vacuum to avoid oxidation, this method becomes impractical. Furthermore, this method is incompatible with measuring angular-dependent emission. Therefore, we chose to measure the emission from the sample directly, and obtain the emittance by comparing the emission from a reference object with known emissivity; this is called the direct method. A common method of heating the sample is by clamping it to a solid, heated block, to achieve an isothermal condition with the block, itself. The temperature of the sample surface is determined by comparison to a characterized reference sample mounted next to the sample under test. However, when a sample is attached directly on top of a solid block it introduces an emitter additional to the photonic crystal and the substrate. Therefore, we chose to heat the sample from the edge, but the inevitable temperature profile across the photonic crystal presents a serious challenge to determining the photonic crystal temperature. In the later part of this paper, we will describe, in detail, the methodology of how this challenge was met and mitigated.

To determine the emissivity of the photonic crystal-substrate system, we consider the photonic crystal and the substrate as two independent isothermal emitters, as shown in Figure 2.1. For the moment we consider the perturbation posed by having one side of the photonic crystal in contact with the silicon substrate to be small allowing their treatment as independent emitters. Later we will show that our experimental results support this model. In this independent emitter model, the effective emission is the sum of the emission from the photonic crystal and the transmitted emission from the silicon substrate. In terms of the effective emissivity (E_{eff}), it is expressed as,

$$E_{eff} = E_{PC} + E_{Si} * T_{PC} = (1 - R_{PC}) + (E_{Si} - 1) * T_{PC}, \qquad (1)$$

where R_{PC} and T_{PC} are the total reflectivity and transmissivity of the free-standing photonic crystal, respectively, E_{PC} and E_{Si} are the emissivity of the photonic crystal and silicon substrate respectively. If the silicon substrate is replaced with a blackbody substrate, equation (1) reduces to the photonic crystal emissivity 1-R_{PC}. On the other hand, if E_{Si} is zero, which is the room temperature case, the E_{eff} is just the absorptivity of the photonic crystal. Therefore, by measuring separately the emissivity of the silicon substrate and the

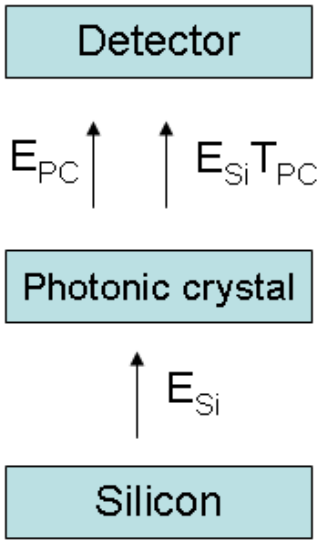

Figure 2.1: Independent emitter model for the photonic crystal-substrate system emission.

photonic crystal-substrate system, we can accurately validate the theoretical prediction of the total reflectivity and transisissivity of the photonic crystal itself. The importance of this equation is that we do not have to measure the total transmittance and reflectance of the substrate or the photonic crystal.

2.3 Experimental methods

The main challenges to any emissivity measurement are: determining the temperature of the sample, and the calibration of the detector gain and spectral response. In addition, stray light entering into the detection system can also introduce error. In this section, we will describe the optical system and calibration procedures used to perform our emissivity measurements. The schematic diagram of the apparatus is shown in Figure 2.2. An off-axis parabolic mirror (152 mm focal length) is used to collect (full collection angle of 19^{o}) and relay image the emission from the sample to an image plane, where an approximately 1.5 mm diameter aperture is placed. The transmitted light is collected and focused by another off-axis parabolic mirror into a mercury cadmium telluride (MCT) detector. The image plane is located in the sample chamber of the FTIR (Fourier Transform Infrared) spectrometer (a Nicolet Nexus 870 with a CaF_2 beamsplitter). The imaging system has a demonstrated 0.5 mm resolution, consistent with the size of the pinhole used. The vacuum Dewar that houses the sample-heater block system is on an x-y translation stage to allow emission measurements to be made on one of the two samples, the blackbody cavities, or any part of the heater block. The imaging system and the fixed aperture maintain a constant sampling area from the sample, and keep stray light from entering into the detector. A background light level without any sample scattered in the vacuum dewar on the order of 1% of the signal

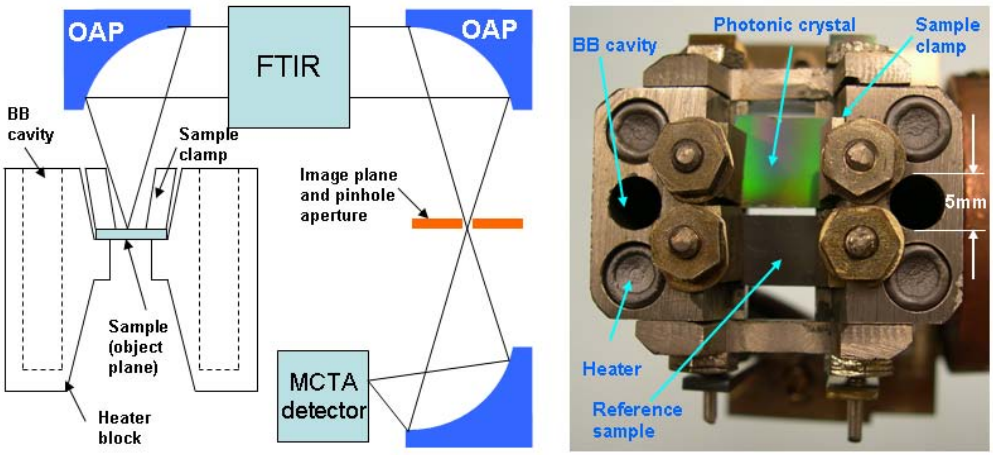

Figure 2.2: Optical system and heater block of the emission experiment. The picture on the right shows the photonic crystal and reference samples mounted next to each other.

from the blackbody cavity. Because the silicon substrate has an emissivity of about 0.7-0.8 at elevated temperatures, this contribution is reduced to 0.3% which far less than other sources of uncertainty.

The sample is heated conductively by the heater block from two sides of the sample, as shown in Figure 2.2. Every component of the heater block, including sample clamps, nuts, washers and threaded rods are made of molybdenum, which remove mismatches in thermal expansion coefficients. The molybdenum construction also allows the sample to be heated to

temperatures substantially beyond 1000 K. Four cylindrical heater cartridges from Watlow (Firerod E1A51-9505) can deliver up to 450W of total power to the block. In the experiments we report here, a total input power of about 100W was used to achieve a heater block temperature of 1000 K.

The heater block has two built-in cylindrical blackbody cavities, each 23 mm deep with a 5 mm diameter. The cavities are coated with high-temperature Aremco HiE840 paint, producing an effective emissivity of 0.97, as measured with the focal plane 6.3 mm into the hole. This effective emissivity is consistent with the calculations by Chandos [19]. Emissions from these cavities are used to determine the heater block temperature, provide an *in situ* emissivity calibration, and serve as a convenient position marker for mapping the temperature profile of the reference and sample under test (SUT). Upon correcting the FTIR-detector system response using a NIST-traceable blackbody source, the temperature of the blackbody cavity in the heater block can be determined to within +/-0.7 K.

Two samples can be mounted on the heater block with independent clamps. One of these samples serves as a reference sample, and the other is the SUT. The reference sample will be used to determine the temperature of the SUT. Because the samples are heated from two ends, they have a parabolic-like temperature profile between the two heat sources. At the center, the temperature gradient is at a minimum at the coldest part of the sample, and is therefore the location at which the emission measurement is taken. Because our sampling spot size is 2mm dia, the measured temperature is an average temperature of the sample over this area. Based on finite element thermal analysis, the average temperature over a 2 mm region where the temperature gradient is at a minimum is 0.07% higher than the temperature

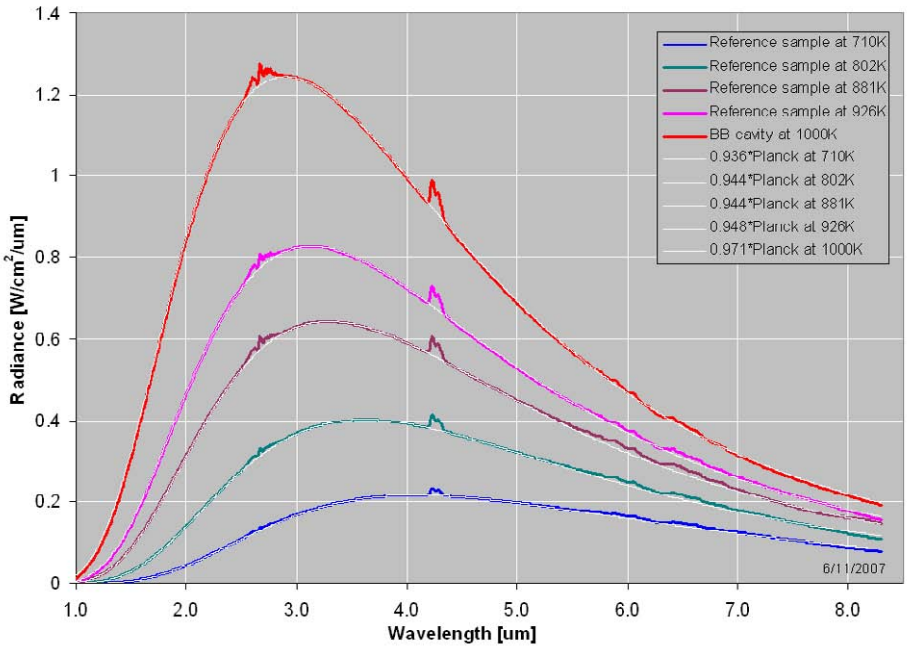

Figure 2.3: Emission from the reference sample at several temperatures, and the left blackbody cavity in the heater block at 1000K. The fitted Planck distribution curves (dashed) are overlaid on top of these curves. The emissivity factor of each curve is shown in the legend. The features that protrude out of the Planck curve are due to small difference in the water absorption from the calibration beam path.

at the minimum point. This error is small, even compared with the temperature uncertainty of the NIST-traceable blackbody source.

In order to determine the temperature of the sample under test, we use the temperature of the reference sample as our thermometer. The reference sample is a piece of silicon with the same thickness as the photonic crystal substrate. It has the same temperature profile as the SUT, due to them having the same heat transfer properties. To ensure the reference sample has a temperature- and wavelength-independent emissivity, a thin film of nitrogen-poor aluminum nitride with a dark-grey matte finish was deposited on the polished side of the silicon surface; this coating is referred as MDL black. Upon coating the MDL black with HiE840 black paint, the material has a stable emissivity of 0.94 +/-0.014 under repeated temperature and vacuum cycling. By replacing the sample under test with a second reference sample, and mapping the temperature along the symmetry line, a small temperature variation caused by the differences in the heater resistances was found. The measured temperature uncertainty at the SUT location is +/-0.3%, and is consistent with our ability to reproducibly position the sample to +/-0.25 mm. At the moment this is the biggest source of error in our emissivity measurements. We believe by controlling the heater voltages independently, this temperature variation on the heater block can be reduced substantially.

2.4 Detector calibration

Detector spectral and nonlinear gain responses are calibrated using a NIST-traceable blackbody source. This is accomplished by rotating the first off-axis parabolic mirror by 90° to collect the light from the blackbody source. To account for the surface reflection loss, and a small amount of water content in the CaF_2 window, this calibration is performed with the exact same window in the beam path. A family of detector response curves is derived by measuring the blackbody source from 493 to 1183K in intervals of 50-30 K. At temperatures not covered by these measurements, a linear interpolation of the two nearest temperatures is used. Figure 2.3 illustrates the validity of this calibration method by comparing the corrected detector signals to a calculated Planck spectrum. The temperature uncertainty of the source in the temperature range of 420-960 K is 1.5-1.7 K. This represents an emissivity uncertainty of +/-0.004 in the 3 μm region. To ensure that all the nonlinear responses have been corrected, we also have to use a nonlinear correction method. The method involves fitting the detector response to a third-order polynomial for each wavelength. These fits have less than one part in 10^4 rms error. The true irradiance from the sample is obtained by finding

Source	Uncertainty (%)
NIST traceable BB source	±0.4
Detector stability	±1.5
Measurement location	±0.3
Temp difference between reference and test sample	±1.4
Total RMS error	±2.0

Table 2.1: Error contributions from calibrated source, detector, measurement location and temperature uncertainty of the test sample.

roots of the cubic equation for each specific wavelength. Experimentally, the measured +/- 0.014 emissivity uncertainty from our built-in blackbody cavity is consistent with the estimated uncertainty from this analysis. However, the temperature uncertainty of the sample due to positioning error, and with respect to the reference sample, is +/-0.3%. A summary of the error contributions is shown in Table 1. Assuming these errors are not correlated, the resulting uncertainty in the emissivity at 3 μm is +/- 0.02. Finally, we determine the emissivity of the blackbody cavity in the heater block to be 0.97+/-0.014, and the reference sample is 0.94+/-0.02.

2.5 Results and discussions

In order to be able to use the reference sample as the temperature monitor for the SUT, it is important that the emissivity of this material be wavelength-independent and stable over time. The emissivity of the reference sample has been measured many times with vacuum and temperature cycling, and there is no noticeable systematic drift in the emissivity value of the reference sample. The spectral dependence of the emissivity of the reference sample is very flat, as shown in Figure 2.4. In the spectral region of 1 to 1.5 μm, the data is not trust worthy because of the poor sensitivity of the MCT detector, which hampers the ability to obtain an accurate correction in this region. The silicon emissivity is also found to be temperature- and wavelength-independent for temperatures of 700-960 K. The silicon sample is an n-type <100> surface with a resistivity value of 0.004-0.04 -cm. The emissivity measured is 0.77+/-0.02, a value slightly higher than the 0.69 reported by Sato and Timan [18, 16, 20, 21]. Sato's samples were polished on both sides. Vandenabeele used a silicon wafer 675 μm thick with varying degrees of roughness on the backside; he measured saturated emissivities of 0.70-0.78 for the different roughnesses [20]. The emissivity of silicon increases with roughness and oxide thickness. Our result is within the range of

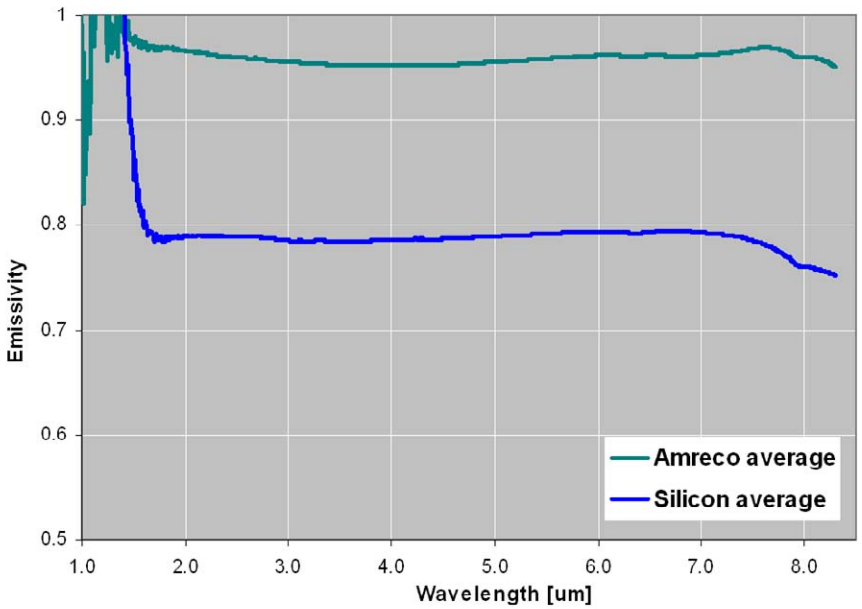

Figure 2.4: Emissivty of the Aremco paint and the silicon wafer. The silicon sample is 680μm thick, with an unpolished backside and a resistivity of 0.004 - 0.04 -cm.

emissivities one expects from roughened silicon and lends confidence to our measurement

methodology. The temperature at which the silicon emissivity saturates is consistent with low resistivity silicon.

The photonic crystal we measured is an 8-layer tungsten logpile photonic crystal with a periodicity of 2.85 μm. The rod width is 0.8 μm, with a height of 1.3 μm. The lowest photonic crystal bandedge occurs at 4.5 μm. The fabrication process [22] and the optical properties of metallic photonic crystals [23] have been discussed in previous publications. If the photonic crystal is free-standing and is heated by a blackbody substrate, then the emissivity is given by 1-R from Eq. 1, which is shown as the brown curve in Figure 2.5. The broad peak that spans from 2.8 to 3.4 μm, and the features at 4.16 and 4.48 μm, are the propagating modes of the photonic crystal. However, because of the presence of a semi-transparent substrate, the emissivity is modified and is given by Eq. 1, according to the independent emitter model. The R and T in Eq. 1 are the calculated total reflectivity and transmissivity of the free standing photonic crystal. For the silicon emissivity we used the measured value of 0.77. This result is shown by the blue curve in Fig. 2.5, using the measured Si emissivity. This model agrees very well with the measured emissivity of the photonic crystal-substrate system (red curve in Fig. 2.5). On the other hand, if the substrate emissivity is assumed 1 (brown curve), the disagreement is very significant (25%).

The deep intensity modulation and sharp features at 4.16 μm and 4.5 μm are only qualitatively reproduced in the experimental measurements. This discrepancy may be due to the angular averaging effect over the full acceptance angle of 19^{o} in our measurements. In addition, fabrication imperfections of the photonic crystal, such as variations in the layer thicknesses, rod dimensions and periodicity may also have some contribution. In the

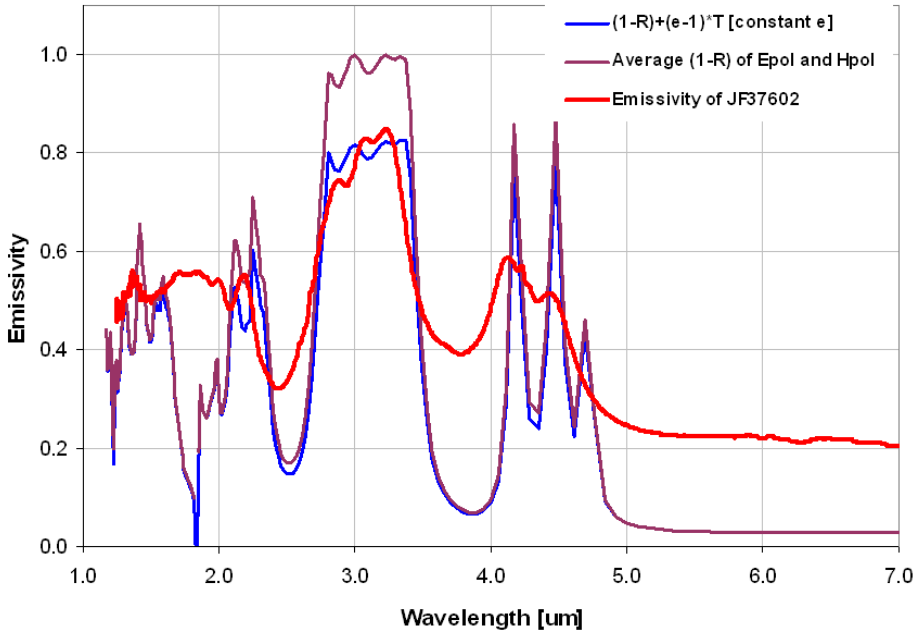

Figure 2.5: Measured emissivity of photonic crystal is compared with independent emitter model. The red trace is the measured emissivity from the photonic crystal-silicon system. The brown curve is the calculated 1-R, where R is the total reflectivity. The blue curve is the calculated (1-R)+(e-1)*T, where e is the emissivity of the silicon, and R and T are the calculated total reflectivity and transmissivity of the photonic crystal. Since the measured emissivity (0.77) of Si very flat in the wavelength region of interest, a constant value of 0.77 was used.

temperature range we investigated, we found no significant temperature dependence in the emissivity. We have measured two other samples from the same wafer, while the overall features are the same there are some subtle difference in spectral details and the depth of modulation. This is believed to be due to non-uniformities in the layer thicknesses across the wafer caused by the chemical mechanical polishing process. None of the three samples we measured showed any indication of the non-equilibrium behavior that Chow predicted [8]. Finally, we wish to point out that in reality, the photonic crystal is built on a very thin layer (800 nm) of non-stoichiometric silicon nitride on the surface of the Si, which is required to bond the W rod to the Si wafer; we believe this effect to be small enough so as not to affect the general conclusions of our measurements. Future investigations will attempt to account for the perturbation introduced by this layer. We believe this work represents the most accurate measure of the photonic crystal emissivity with a maximum uncertainty of +/-0.02.

2.6 Summary

In summary, we have developed an accurate methodology to measure photonic crystal emissivity using a direct method. The method requires measuring two quantities: the total emissivity of the photonic crystal-substrate system, and the emissivity of the substrate alone. An independent emitter model was developed to relate the reflectance and transmittance of bare photonic crystal to the measured quantities. This method addresses the photonic crystal substrate effect when compare with theoretical calculations. The measured results agree very well with this independent emitter model. Our measurements have an uncertainty of 4% and represent the most accurate measure of a photonic crystal's emissivity. Furthermore, these measurements also show no indication of non-equilibrium behavior.

2.7 References

[1] Joannopoulos J.D., Meade R.D. and Winn J.N., *Photonic Crystals*, Princeton University Press, Princeton, 1995.

[2] Lin S.Y., Fleming J.G., and El-Kady I., "Three-dimensional photonic-crystal emission through thermal excitation", *Opt. Lett.*, **28**, 1909 (2003).

[3] Lin S.Y., Moreno J., Fleming J.G., "Three-dimensional photonic-crystal emitter for thermal photovoltaic power generation", *Appl. Phys. Lett.*, **83**, 380 (2003).

[4] Lin S.Y., Fleming J.G. and El-Kady, I, "Highly efficient light emission at λ=1.5 μm by a three-dimensional tungsten photonic crystal", *Opt. Lett.*, **28**, 1683 (2003).

[5] Cornelius C.M. and Dowling J.P., "Modification of Planck blackbody radiation by photonic band-gap structures", *Phys. Rev. A*, **59**, 4736 (1999).

[6] Florescu M., Busch K., Dowling J.P., "Thermal radiation in photonic crystals", *Phys. Rev. B*, **75**, 201101(R), (2007).

[7] El-Kady I., Chow W.W. and Fleming J.G., "Emission from an active photonic crystal", *Phys. Rev. B*, **72**, 195110 (2005).

[8] Chow W.W., "Theory of emission from an active photonic lattice", *Phys. Rev. A*, **73**, 013821 (2006).

[9] Luo C., Narayanaswamy A., Chen G. and Joannopoulos J.D., "Thermal Radiation from Photonic Crystals: A Direct Calculation", *Phys. Rev. Lett.*, **93**, 2139051 (2004).

[10] Chan D.L.C., Soljacic M. and Joannopoulos J.D., "Direct calculation of thermal emission for three-dimensionally periodic photonic crystal slabs", *Phys. Rev. E*, 74, 036615 (2006).

[11] Snyder W.C., Wan Z. and Li X., "Thermodynamic constraints on reflectance reciprocity and Kirchhoff's law", *Appl. Opt.*, 74, 3464 (1998).

[12] Trupke T., Wurfel P., and Green M.A., "Comment on ''Three-dimensional photonic-crystal emitter for thermal photovoltaic power generation", *Appl. Phys. Lett.*, **84**, 1997 (2004).

[13] Greffet J.J., Nieto-Vesperinas M., "Field theory for generalized bidirectional reflectivity: derivation of Helmholtz's reciprocity principle and Kirchhoff's law", *J. Opt. Soc. Am. A*, **15**, 2735 (1998).

[14] Lin S.Y., Moreno J., and Fleming J.G., "Response to ''Comment on Three-dimensional photonic-crystal emitter for thermal photovoltaic power generation' '' .Appl. Phys. Lett. 84, 1997 .2004.. *", Appl. Phys. Lett.*, **84**, 1999 (2004).

[15] Seager C.H., Sinclair M.B., and Fleming J.G., "Accurate measurements of thermal radiation from a tungsten photonic lattice", *Appl. Phys. Lett.*, **86**, 244105 (2005).

[16] Sato T., "Spectral Emissivity of Silicon", *Jap. J. of Appl. Phys.*, **6**, 339 (1968).

[17] McMahon H.O., "Thermal Radiation from Partially Transparent Reflecting Bodies", *J. of Opt. Soc. Am.*, **40**, 376 (1950).

[18] Chubb D.L., Wolford D.S., Meulenberg A. and DiMatteo R.S., "Semiconductor Silicon as a Selective Emitter", *AIP conference proceedings* **653**, 174 (2003).

[19] Chandos R.J. and Chandos R.E., *Appl. Optics*, **13**, 2142 (1974).

[20] Vandenabeele P. and Maex K., "Influence of temperature and backside roughness on the emissivity of Si wavers during rapid thermal processing", *J. of Appl. Phys.*, **72**, 5867 (1992).

[21] Timan P.J., "Emissivity of silicon at elevated temperatures", *J. of Appl. Phys.*, **74**, 6353 (1993).

[22] Fleming J.G., Lin S.Y., El-Kady I., Biswas R., and Ho K.M., "All-metallic three-dimensional photonic crystals with a large infrared bandgap"**,** *Nature*, **417**, 52 (2002).
[23] Lin S.Y., Fleming J.G., Li , El-Kady I., Biswas R. and Ho K.M., *J. Opt. Soc. Am. B*, **20**,

3. Calculating the dispersion relation for periodic structures using the real-space-based transfer matrix method

3.1 Introduction

Photonic band-gap structures have gained a high interest in the last decade due to their ability to control and confine light propagation [1]. At the turn of the century, there is a possibility that photonic devices may take over the role that electronic devices now have in our life. Due to the high frequency nature of light, the available bandwidth of photonic devices is much higher than conventional electronic devices can provide.

The TMM is one of the most versatile techniques used to calculate the transmission and reflection coefficients of photonic band structures. It models a periodic structure as infinitely periodic stacked layers of its primitive cell (see Figure 3.1). The electromagnetic fields propagate, spatially, in the stacking direction. This allows building the so-called transfer matrix *T* that relates the fields on the entrance and exit faces of a given structure. Most of the work based on this technique was initially developed in [3]-[5], however the method proved only stable for 2D structures.

Previously, most of the work, done in calculating 3D photonic structures, was based on the plane-wave method (PWM). In this method, the frequency is calculated as a function of the propagation constant k, $\omega = f(k)$. In many cases, this limits the capability of modeling frequency dependent materials especially when the modeled structure is susceptible to frequency variations. Unlike the PWM, the real-space-based TMM, combined with Bloch's Theorem, reformulates the problem in a way that the propagating modes are calculated as a function of frequency. This paper is arranged as follows: In section II, the theoretical basis of the real-space TMM scheme is elaborated. Then in section III, the scheme is applied on 2D and 3D lattice structures to calculate the dispersion relation. The results are verified against published and measured data.

3.2 Theory

As a first step, Maxwell's equations are discretized in space by means of finite differences [3]. To accomplish this, the first order Taylor expansion for the propagation term $e^{j\underline{k}\cdot\underline{r}}$ is used:

$$\begin{aligned} k_x &\approx \left(e^{jk_x a} - 1\right) \Big/ (ja), \\ k_y &\approx \left(e^{jk_y b} - 1\right) \Big/ (jb), \\ k_z &\approx \left(e^{jk_z c} - 1\right) \Big/ (jc), \end{aligned} \tag{1}$$

$$
\begin{aligned}
-k_x &\approx \left(e^{-jk_x a}-1\right)\big/(ja),\\
-k_y &\approx \left(e^{-jk_y b}-1\right)\big/(jb),\\
-k_z &\approx \left(e^{-jk_z c}-1\right)\big/(jc).
\end{aligned}
\tag{2}
$$

Then, by applying a Fourier transformation on Maxwell's equations and rearranging terms we can show

$$
\begin{aligned}
E_x(\underline{r}+\underline{c}) &= E_x(\underline{r}) + jc\omega\mu_0\mu_r(\underline{r})H_y(\underline{r})\\
&+ j\frac{c}{a\omega\varepsilon_0\varepsilon_r(\underline{r})}\begin{pmatrix}\left(H_y(\underline{r}-\underline{a})-H_y(\underline{r})\right)\big/a\\ -\left(H_x(\underline{r}-\underline{b})-H_x(\underline{r})\right)\big/b\end{pmatrix}\\
&- j\frac{c}{a\omega\varepsilon_0\varepsilon_r(\underline{r}+\underline{a})}\begin{pmatrix}\left(H_y(\underline{r})-H_y(\underline{r}+\underline{a})\right)\big/a\\ -\left(H_x(\underline{r}+\underline{a}-\underline{b})-H_x(\underline{r}+\underline{a})\right)\big/b\end{pmatrix}
\end{aligned}
\tag{3}
$$

$$
\begin{aligned}
E_y(\underline{r}+\underline{c}) &= E_y(\underline{r}) - jc\omega\mu_0\mu_r(\underline{r})H_x(\underline{r})\\
&+ j\frac{c}{b\omega\varepsilon_0\varepsilon_r(\underline{r})}\begin{pmatrix}\left(H_y(\underline{r}-\underline{a})-H_y(\underline{r})\right)\big/a\\ -\left(H_x(\underline{r}-\underline{b})-H_x(\underline{r})\right)\big/b\end{pmatrix}\\
&- j\frac{c}{b\omega\varepsilon_0\varepsilon_r(\underline{r}+\underline{b})}\begin{pmatrix}\left(H_y(\underline{r}-\underline{a}+\underline{b})-H_y(\underline{r}+\underline{b})\right)\big/a\\ -\left(H_x(\underline{r})-H_x(\underline{r}+\underline{b})\right)\big/b\end{pmatrix}
\end{aligned}
\tag{4}
$$

$$H_x\left(\underline{r}+\underline{c}\right)=H_x\left(\underline{r}\right)-jc\omega\varepsilon_0\varepsilon_r\left(\underline{r}+\underline{c}\right)E_y\left(\underline{r}+\underline{c}\right)$$
$$+j\frac{c}{a\omega\mu_0\mu_r\left(\underline{r}-\underline{a}+\underline{c}\right)}$$
$$\begin{pmatrix}\left(E_y\left(\underline{r}+\underline{c}\right)-E_y\left(\underline{r}-\underline{a}+\underline{c}\right)\right)/a\\-\left(E_x\left(\underline{r}-\underline{a}+\underline{b}+\underline{c}\right)-E_x\left(\underline{r}-\underline{a}+\underline{c}\right)\right)/b\end{pmatrix} \quad (5)$$
$$-j\frac{c}{a\omega\mu_0\mu_r\left(\underline{r}+\underline{c}\right)}$$
$$\begin{pmatrix}\left(E_y\left(\underline{r}+\underline{a}+\underline{c}\right)-E_y\left(\underline{r}+\underline{c}\right)\right)/a\\-\left(E_x\left(\underline{r}+\underline{b}+\underline{c}\right)-E_x\left(\underline{r}+\underline{c}\right)\right)/b\end{pmatrix}$$

$$H_y\left(\underline{r}+\underline{c}\right)=H_y\left(\underline{r}\right)+jc\omega\varepsilon_0\varepsilon_r\left(\underline{r}+\underline{c}\right)E_x\left(\underline{r}+\underline{c}\right)$$
$$+j\frac{c}{b\omega\mu_0\mu_r\left(\underline{r}-\underline{b}+\underline{c}\right)}$$
$$\begin{pmatrix}\left(E_y\left(\underline{r}+\underline{a}-\underline{b}+\underline{c}\right)-E_y\left(\underline{r}-\underline{b}+\underline{c}\right)\right)/a\\-\left(E_x\left(\underline{r}+\underline{c}\right)-E_x\left(\underline{r}-\underline{b}+\underline{c}\right)\right)/b\end{pmatrix} \quad (6)$$
$$-j\frac{c}{b\omega\mu_0\mu_r\left(\underline{r}+\underline{c}\right)}$$
$$\begin{pmatrix}\left(E_y\left(\underline{r}+\underline{a}+\underline{c}\right)-E_y\left(\underline{r}+\underline{c}\right)\right)/a\\-\left(E_x\left(\underline{r}+\underline{b}+\underline{c}\right)-E_x\left(\underline{r}+\underline{c}\right)\right)/b\end{pmatrix}$$

We can rewrite the four equations of (3, 4, 5 and 6) in a matrix form as follows

$$\sum_{\underline{r}'}\begin{bmatrix} T_{11}(\underline{r},\underline{r}') & T_{12}(\underline{r},\underline{r}') & T_{13}(\underline{r},\underline{r}') & T_{14}(\underline{r},\underline{r}') \\ T_{21}(\underline{r},\underline{r}') & T_{22}(\underline{r},\underline{r}') & T_{23}(\underline{r},\underline{r}') & T_{24}(\underline{r},\underline{r}') \\ T_{31}(\underline{r},\underline{r}') & T_{23}(\underline{r},\underline{r}') & T_{33}(\underline{r},\underline{r}') & T_{34}(\underline{r},\underline{r}') \\ T_{41}(\underline{r},\underline{r}') & T_{24}(\underline{r},\underline{r}') & T_{34}(\underline{r},\underline{r}') & T_{44}(\underline{r},\underline{r}') \end{bmatrix} \begin{bmatrix} \underline{E}_x(\underline{r}) \\ \underline{E}_y(\underline{r}) \\ \underline{H}_x(\underline{r}) \\ \underline{H}_y(\underline{r}) \end{bmatrix} = \begin{bmatrix} \underline{E}_x(\underline{r}+\underline{c}) \\ \underline{E}_y(\underline{r}+\underline{c}) \\ \underline{H}_x(\underline{r}+\underline{c}) \\ \underline{H}_y(\underline{r}+\underline{c}) \end{bmatrix} \tag{7}$$

where $T_{mn}(\underline{r},\underline{r}')$ is an n_x x n_y matrix that relates the values of each field component, at a given meshing plane of size n_x x n_y, to the corresponding values at the next adjacent plane. The *T* matrix models a unit cell of the crystal lattice, where an infinite periodicity is assumed in the transverse plane.

By invoking Bloch's theorem in the direction of propagation, equation (7) can be presented as an eigen equation:

$$\begin{bmatrix} \underline{E}_x(\underline{r}+\underline{c}) \\ \underline{E}_y(\underline{r}+\underline{c}) \\ \underline{H}_x(\underline{r}+\underline{c}) \\ \underline{H}_y(\underline{r}+\underline{c}) \end{bmatrix} = T \begin{bmatrix} \underline{E}_x(\underline{r}) \\ \underline{E}_y(\underline{r}) \\ \underline{H}_x(\underline{r}) \\ \underline{H}_y(\underline{r}) \end{bmatrix} = \lambda_i \begin{bmatrix} \underline{E}_x(\underline{r}) \\ \underline{E}_y(\underline{r}) \\ \underline{H}_x(\underline{r}) \\ \underline{H}_y(\underline{r}) \end{bmatrix} = e^{jk_{z,i}C} \begin{bmatrix} \underline{E}_x(\underline{r}) \\ \underline{E}_y(\underline{r}) \\ \underline{H}_x(\underline{r}) \\ \underline{H}_y(\underline{r}) \end{bmatrix} \tag{8}$$

where *T* is the overall transfer matrix of dimensions $4n_xn_y$ by $4n_xn_y$, λ_i is the $i^{\underline{th}}$ eigenvalue of *T*, and $k_{z,i}$ is the corresponding wave number. From equation (8) one can calculate the propagating modes at a given frequency from the eigenvalues of *T*.

Though the real-space based TMM is a straightforward method, it suffers from numerical instability at some point [6]. To analyze this problem, let us go back to the eigenvalue equation:

$$T.F_i = \mathrm{e}^{\pm \mathrm{j}k_{\mathrm{ic}}} F_i \tag{9}$$

where *Fi* is the right-eigenvector. As mentioned before, not all the eigenvalues of *T* present propagating modes. Therefore, not all of the k_i's are pure real values. The nonphysical wavenumbers should have a complex form: $k_{i,re} + j\, k_{i,im}$. For a forward propagating wave, the imaginary term $k_{i,im}$ will cause a numerical exponential growth in the evanescent modes. This error grows as the field propagates through the structure. At some point, these numerical

evanescent modes dominate the propagating ones leading to numerical instability. There are some schemes proposed to overcome this instability [7]. One of the schemes that were proposed is the multi scattering technique. It was proposed by Pendry in [4] and A. Ward in [6]. They applied a unitary transformation S on the transfer matrix T. The S matrix is constructed by summing the multiplications of the left and right eigenvectors of T. However, because of the non-Hermitian nature of T, the proposition that there exists a unitary transformation matrix S, which diagonalizes T, is wrong from the mathematical point of view. To be able to unitarily diagonalize a matrix, it has to be what is known as a normal matrix [8]. A normal matrix A has to satisfy the following identity $A^TA = AA^T$. The T matrix does not satisfy this identity. We constructed a different transformation matrix S for T, which does not have to be unitary, and satisfies the requirements to find the band structure, transmission coefficient, and reflection coefficient for our model.

$$\tilde{T} = S^{-1}TS \tag{10}$$

Under the transformation S, the original bases e_i are transformed to v_i, the eigenvectors of T, where e_i is a column vector with zero elements expect the i^{th} row that has a value of 1. Such a transformation S has to take the following form:

$$S = \begin{bmatrix} | & & | & & | \\ v_1 & \cdots & v_i & \cdots & v_{4\times n_x \times n_y} \\ | & & | & & | \end{bmatrix} \tag{11}$$

In other words, we constructed S in a way that the fields' vector is transformed to a vector that contains the magnitudes of the incident and reflected waves.

3.3 Worked Examples

In this section, the real-space based transfer matrix method is employed to calculate the dispersion relation for 2D and 3D PBG structures. Based on the scheme of $k_z = f(k_x, k_y, \omega)$, the scheme was carried out on the high symmetry axis Γ-X-M-R. Γ, X, M, and R are symmetry points at ⟨000⟩, ⟨001⟩, ⟨011⟩, and ⟨111⟩, respectively. To calculate the dispersion relation in a specific direction, the structure has to be rotated so that the required direction coincides with the z-axis. Also, any rotational symmetry is utilized to simplify calculations in symmetrical structures.

Example 1

The structure to be modeled is a 2D periodic structure of an array of alumina rods embedded in air as shown in Figure 3.1:. Alumina exhibits a low loss relative permittivity of around 9 from 15-135 GHz [9]. The spacing is 2.4 mm, and the cylinder diameter is 2.16 mm. This structure was experimentally measured using the coherent microwave transient spectroscopy (COMITS) technique [9]. The measured dispersion relation for the TE mode and TM modes are plotted as solid circles and squares in Figure 3.2 and Figure 3.3, respectively.

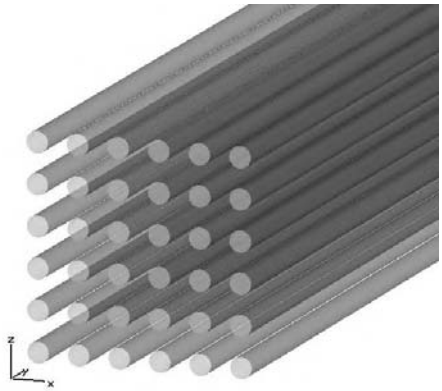

Figure 3.1: An infinite periodic array of cylindrical alumina rods, $_r$ = 9. The radius of the cylinder is 1.08 mm and the lattice constant a = 2.4 mm.

As for the TMM calculations, the unit cell is discretized to 13x1x13 meshing points. There is only one meshing point in the y-direction due to the invariant permittivity along the y-axis. This implies that the transfer matrix has a size of 52x52. The calculated dispersion relation for the TE and TM modes is shown in Figure 3.2 and Figure 3.3, respectively. The plots show a strong agreement between the calculated and measured data [9].

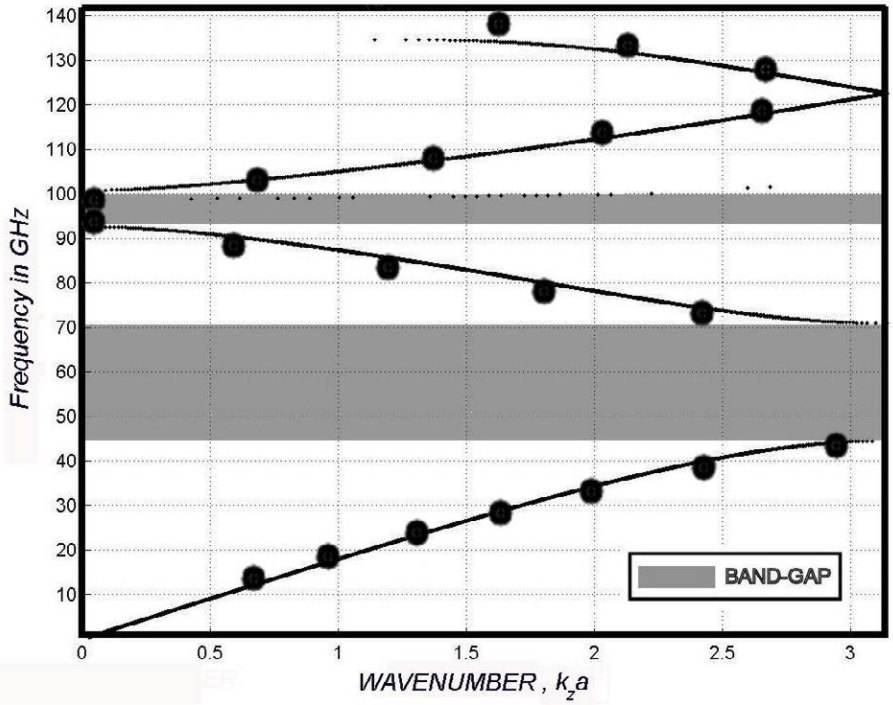

Figure 3.2: The dispersion relation of the TE-mode calculated for the two-dimensional alumina rod structure shown in Figure 3.1:. The measured data is plotted as solid circles [9].

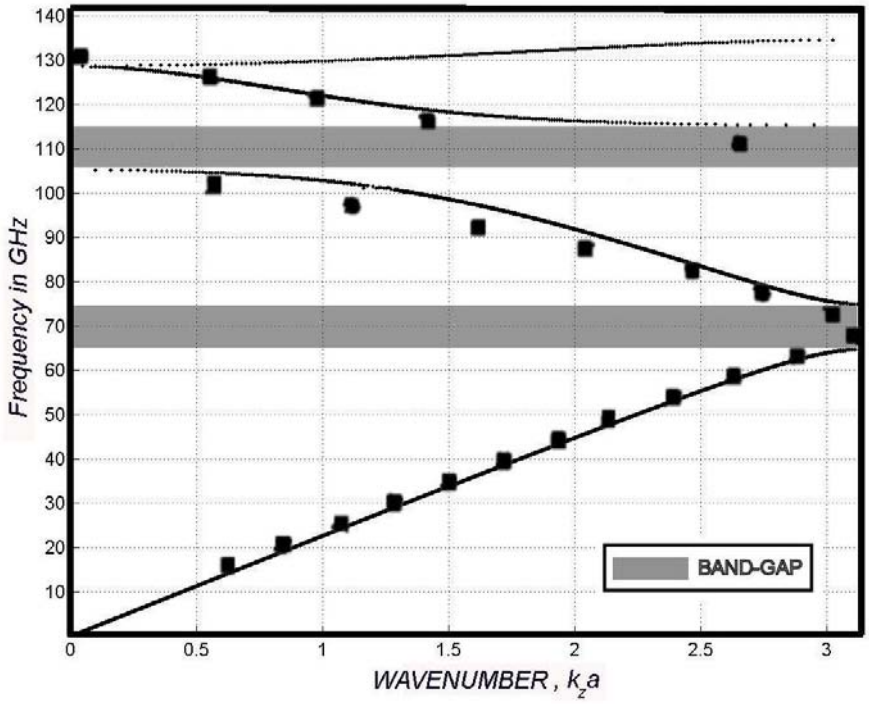

Figure 3.3: The dispersion relation of the TM-mode calculated for the two-dimensional alumina rod structure shown in Figure 3.1:. The measured data [9] is plotted as solid squares [9].

Example 2

This example is a simple cubic lattice of dielectric spheres embedded in air as shown in Figure 3.4. The spheres have a dielectric constant of 11.56, and radius of 0.3*a*, where *a* is the lattice constant [11]. The unit cell is discretized to10x10x10 meshing points. This yields a transfer matrix of size of 400x400.

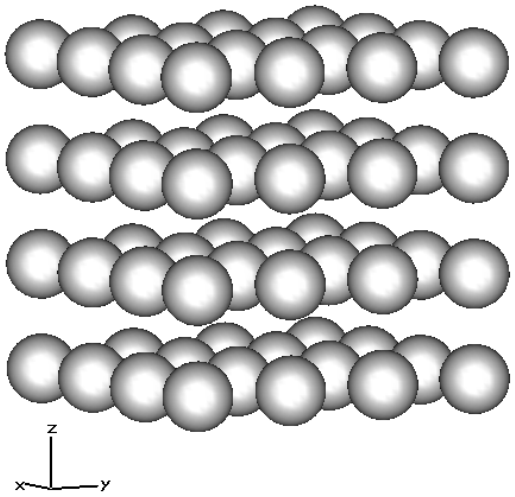

Figure 3.4: 3D simple cubic lattice of dielectric spheres embedded in air. The dielectric constant ε_r = 11.56, and the radius of each sphere $r = 0.3a$, where *a* is the lattice constant.

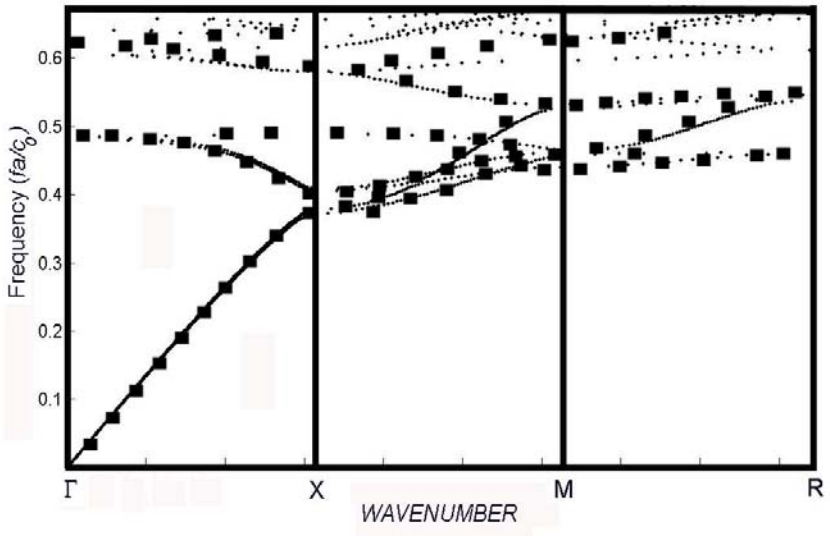

Figure 3.5: The calculated full band structure using the real-space-based TMM. The solid squares present the data obtained by the plane-wave-based TMM [12].

It is apparent that the modeled lattice does not exhibit a full band-gap, as explained in [2]. However, it has a directional band-gap along Γ-X. For verification purposes, our results were compared to the calculated dispersion relation using the plane-wave-based TMM in [12]. The real-space-based TMM calculated a directional band-gap between frequencies 0.3797(c_0/a) and 0.4080(c_0/a), where c_0 is the speed of light in free space. As for the calculation by means of the plane-wave based TMM, the directional band-gap is lying between frequencies of 0.38(c_0/a) and 0.412(c_0/a). The difference between the two is less than 1%. Also, Figure 3.5: shows a perfect matching between the results of both methods.

Example 3

The next structure is a 3D simple cubic lattice structure as shown in Figure 3.6. The dielectric square rods are made out of silicon with a width of 0.8 μm. The lattice constant *a* is 3.2 μm **Error! Reference source not found.**.

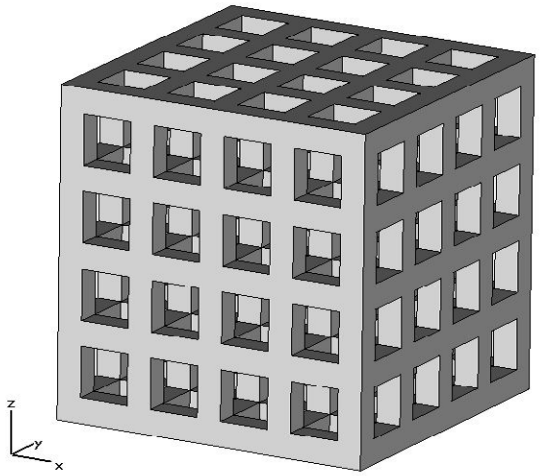

Figure 3.6: 3D cubic lattice of dielectric square rods. The rod has a width of 0.8 m and relative permittivity of 12.96. The lattice constant a = 3.2 m.

The dispersion relation for the structure shown above is calculated by means of the real-space-based TMM. The results are plotted in Figure 3.7:. The calculated data shows excellent agreement with previous published data **Error! Reference source not found.** which is presented by solid squares in Figure 3.7:. It is apparent that this structure exhibits a complete band-gap between frequencies of 0.378(c_0/a) and 0.383(c_0/a).

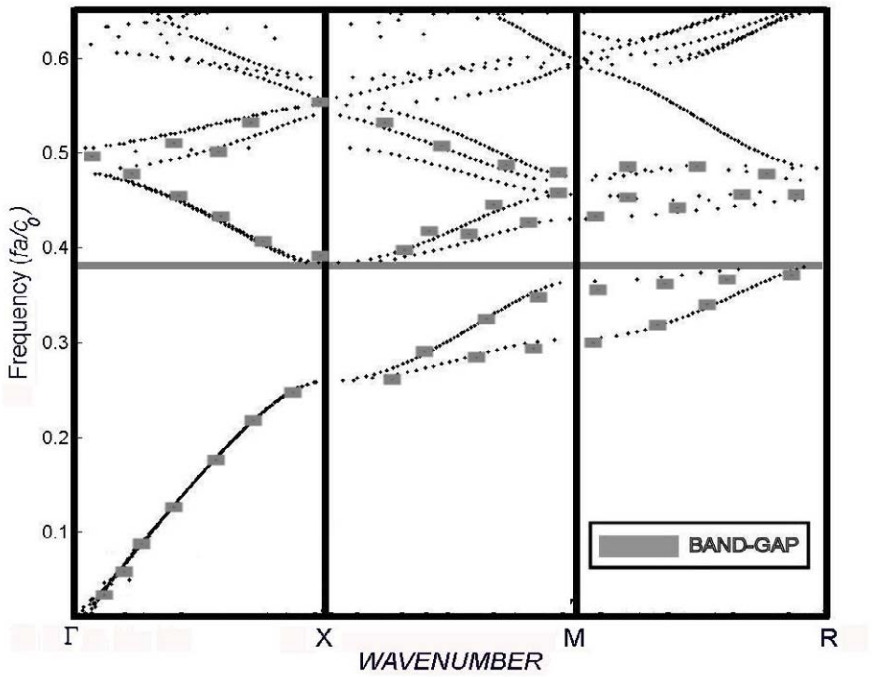

Figure 3.7: The calculated dispersion relation for the structure in Figure 3.6. Data published in is plotted as solid squares **Error! Reference source not found.**.

3.4 Conclusions

The transfer matrix method (TMM) utilizing a real-space basis combined with Bloch's theorem is used to calculate the dispersion relation for lossless periodic materials. The TMM method is characterized by its capability to model frequency dependent materials. Also, it can handle negative index materials without any further complications in coding. The entire code has been implemented in MATLAB and it can handle frequency dependent dielectric materials that comprise the photonic crystal. In this work, the real-space-based TMM is applied to 2D and 3D periodic structures. Comparisons between this approach with measured and published data show a perfect match in results.

3.5 References

[1] E. Yablonovitch, "Inhibited Spontaneous Emission in Solid-State Physics and Electronics," Phys. Rev. Lett. **58**, 2059, 1987.

[2] J. Joannopoulos, R. Meade, and J. Winn, "Photonic Crystals," Princeton U. Press, Princeton, N.J., 1995.

[3] J.B. Pendry, "Photonic Band Structures," J. Mod. Opt. **41**, 209-229, 1994.

[4] J.B. Pendry, "Calculating Photonic Band Structures," J. Phys. Condensed Matter **8**, 1085-1108, 1996.

[5] P.M. Bell, J.B. Pendry, L.M. Moreno, and A.J. Ward, " A program for calculating photonic band structures and transmission coefficients of complex structures," Comp. Phys. Comm. **85,** 306-322, 1995.

[6] A. J. Ward, " Transfer Matrices, Photonic Bands and Related Quantities," PhD Thesis, university of London, Condensed Matter Theory Group, Imperial College of Science, Technology and Medicine, London, July 1996.

[7] B. Gralak, S. Enoch, and G. Tayeb, "From scattering or impedance matrices to Bloch modes of photonic crystals," J. Opt. Soc. Am. A, **19**, No. 8, August 2002.

[8] G. Strang, "Linear Algebra and Its Applications," 3rd Ed., Brooks Cole, 1988.

[9] W.M. Robertson and G. Arjavalingam, R. D. Meade, K. D. Brommer, A. M. Rappe, and J.D. Joannopoulos, "Measurement of Photonic Band Structures in a Two- Dimensional Periodic Dielectric Array, " Phys. Rev. Lett., **68**, Num. 13, Mar 1992.

[10] S. Y. Lin, G. Arjavalingam, and W. M. Robertson, "Investigation of Absolute Photonic Band Gaps in Two-Dimensional Dielectric Structures," J. Mod. Opt. **41**, 385-393, 1994.

[11] M. Armanious, C. Christodoulou, and I. El-Kady, "Calculating Photonic Band Structures Using The Transfer Matrix Technique," IEEE AP/URSI Symp. Washington, DC, 2005.

[12] Z.-Y. Li and L.-L. Lin, "Photonic band structures solved by the plane-wave-based transfer-matrix method," Phys. Rev. E **67**, 046607, 2003.

[13] S.-Y. Lin, J.G. Fleming, and R. Lin, "Complete three-dimensional photonic bandgap in a simple cubic structure," J. Opt. Soc. Am. B **18**, No. 1, 2001.

4. Accomplishments

4.1 Refereed Publications resulted from this project

1. El-Kady, I., W. W. Chow, J. G. Fleming, *Emission from an Active Photonic Crystal*' Phys. Rev. B. **72**,195110 - 5 , 2005.

2. M. F. Su, **I. El-Kady**, and C. G. Christodoulou,"*Calculating Photonic Band Structure Using the Transfer Matrix Technique*", IEEE AP-S International Symposium and USNC/URSI National Radio Science Meeting proceedings, (2005).

3. W. W. Chow, 'Theory of emission from an active photonic lattice,' Phys. Rev. A **73**, 013821-9. 2006.

4. Chow, W. W., I. Waldmueller, *Active Photonic Lattices: Is Greater than Blackbody Intensity Possible?*, Journal of Modern Optics 53, 2371 (2006).

5. T.S. Luk, T. McLellan, G. Subramania, J.C. Verley, and I. El-Kady, *Emissivity measurements of 3D photonic crystals at high temperatures,* revised manuscript submitted to Photonics and Nanostructures – Fundamentals and Applications (special issue) (2007).

6. Farfan, B.G., Rammohan, R., Su, M. F., **El-Kady, I.** and Reda Taha, M. M. "Prediction of Photonic Crystals Emitter Efficiency Using An Optimized Fuzzy Learning Approach", *Photonic and Nanostructures – Fundamentals and Applications*, (Submitted August 2007).

7. Rammohan, R., Farfan, B.G., Su, M. F. Reda Taha, M. M., and **El-Kady, I.** "A Guided Semi-Natural Genetic Optimization for Smart Design of Photonic Crystal Filters", *Engineering Application of Artificial Intelligence*, (Submitted August 2007).

4.2 Conference Proceedings resulted from this project

1. I. El-Kady, T.S. Luk, W. Sweatt, "Smart Design of IR Scene Generation Using Metallic Photonic Crystals", *Photonic and Electromagnetic Crystal Structures VII (PECS-VII)*, Monterey, CA, April 2007.

2. M. F. Su, I. El-Kady, E. A. Shaner, and C. G. Christodoulou, "Selective Enhancement of Mid-IR Quantum Dot Electroluminescent Emissions Using Defect Mode Photonic Crystal Cavities", *IEEE AP Symposium* in Honolulu, Hawaii, June 2007.

3. I. El-Kady, M. F. Su, J.G. Fleming, R. H. Olsson III, and T.S. Luk, "Modeling of micromachined acoustic bandgap structures and devices", *Photonic and Electromagnetic Crystal Structures VII (PECS-VII)*, Monterey, CA, April 2007.

4. I. El-Kady, C. Murray, T.-S. Luk, R. Koudelka, J. G. Fleming, "*Photonic Crystal Assisted High-Efficiency Thermal Photovoltaic Generation"*, Conference on Lasers and Electro-Optics (CLEO), Conference Proceedings, In print (2006)

5. I. El-Kady, W. Chow and J. Fleming, "*Thermal Emission from an active metallic photonic crystal*", PECS-VI International Symposium on Photonic and Electromagnetic Crystal Structures Proceedings, (2005).

6. C. Murray, J. Fleming, R. Koudelka, and I. El-Kady, "*Improved Thermophotovoltaic Energy Conversion with 3-D Tungsten Photonic Crystal*", PECS-VI International Symposium on Photonic and Electromagnetic Crystal Structures Proceedings, (2005).

7. M. Armeneous, C. Christodulo, and I. El-Kady, "*Calculating Photonic Band Structure Using the Transfer Matrix Technique*", IEEE AP-S International Symposium and USNC/URSI National Radio Science Meeting proceedings, (2005).

8. I. El-Kady and J.G. Fleming, "*Photonic Crystals: From a Nano-size Scientific Novelty to Realizable Hi-Tech. Applications"*, Nano-Tech Insight conference proceedings, (2005).

4.3 Invite Presentations resulted from this project

1. I. El-kady, W. W. Chow, 'Emission from an active photonic lattice: does it exceed the blackbody's?' Colloquium on the Physics of Quantum Electronics, 1/2-6/05, Snowbird, UT (invited).

2. I. El-Kady, J. Fleming, 'Photonic Crystals: From a Nano-size Scientific Novelty to Realizable Hi-Tech. Applications', Nano-Tech conference, 2/05 Luxur, Egypt UT (invited).

3. W. W. Chow, 'Emission from an active photonic lattice: does it exceed the blackbody's?' Photonic Seminar, Electrical and Computer Engineering Dept, University of Illinois, 4/27/05, Urbana-Champaign, IL (invited).

4. I. El-Kady, J. Fleming, C. W. Chow 'Photonic Crystals Science and Applications', IGERT Colloquium 8/05 UNM (invited).

5. Chow, W. W., *Emission from an Active Photonic Lattice: Is Greater than Blackbody Intensity Possible?,* Seminar at College of Optical Sciences, University of Arizona, 10/31/06, Tucson, AZ (invited).

6. Chow, W. W., *Emission from an Active Photonic Lattice: Is Greater than Blackbody Intensity Possible?* LASERION 2007 Workshop, 7/1-6/07, Ringberg, Germany (invited).

7. T.S. Luk, *Absolute emissivity measurements of 3D photonic crystal,* SPIE Optics and Photonics, Aug. 26-30, 2007, San Diego, CA. (invited).

4.4 Contributed Conference Presentations resulted from this project

1. W. W. Chow, 'Emission from photonic crystals: Does it exceed the blackbody's?', Nanotechnology Symposium, Quantum Science Research, Hewlett-Packard Laboratories, March 25, 2005, Palo Alto, Ca.

2. W. W. Chow, 'Emission from an active photonic lattice: does it exceed the blackbody's?' Palo Alto Research Center (PARC), 5/17/05, Palo Alto, CA

3. I. El-Kady, J. Fleming, Thermal Emission from an active metallic photonic crystal", PECS-VI, Aghia Pellaghia, Crete, Greece, 2005.

4. W. W. Chow, 'Emission from an active photonic lattice: is greater than blackbody intensity possible?' Theoretical Physics Colloquium, Technical University, 11/8/05, Kaiserslautern, Germany.

5. W. W. Chow, 'Emission from an active photonic lattice: is greater than blackbody intensity possible?' Berkeley Optoelectronics Seminar Series, UC Berkeley EECE, 12/2/05, Berkeley, CA.

6. W. W. Chow, 'Active photonic lattices: is greater than blackbody intensity possible?' 36th Winter Colloquium on the Physics of Quantum Electronics, 1/2-6/06, Snowbird, UT.

7. W. W. Chow, I. El-Kady, 'Emission from an active photonic lattice: does it exceed that of the blackbody?' SPIE Photonic West Conference, 1/23-27/06, San Jose, CA.

8. W. W. Chow, 'Microscopic theory of optical response: from thermal emission of photonic crystals to many-body effects in semiconductor lasers,' Physics Department Colloquium, Texas A&M University, 4/25/06, College Station, TX.

9. I. El-Kady, C. Murray, T.S. Luk, R. Koudelka W. Chow, and J. G. Fleming 'Photonic Crystal Assisted High Efficiency Photovoltaic Generation', CLEO, 5/21-26/06,Long beach,CA

10. Chow, W. W., *Emission from an Active Photonic Lattice: Is Greater than Blackbody Intensity Possible?*,Seminar at Technische Universitat Berlin, 12/5/06, Berlin, Germany (invited).

11. M. F. Su, I. El-Kady, E. A. Shaner, and C. G. Christodoulou, "Selective Enhancement of Mid-IR Quantum Dot Electroluminescent Emissions Using Defect Mode Photonic Crystal Cavities", *IEEE AP Symposium* in Honolulu, Hawaii, June 2007.

12. I. El-Kady, C. Murray, T.-S. Luk, R. Koudelka, J. G. Fleming, *"Photonic Crystal Assisted High-Efficiency Thermal Photovoltaic Generation"*, Conference on Lasers and Electro-Optics (CLEO), Conference Proceedings, In print (2006)

13. M. Armeneous, C. Christodulo, and I. El-Kady, "*Calculating Photonic Band Structure Using the Transfer Matrix Technique*", IEEE AP-S International Symposium and USNC/URSI National Radio Science Meeting proceedings, (2005).

Distribution

MS 1082	James Hudgens	01725
MS 1082	Frederick Mccormick	01727
MS 1082	Ihab El-Kady	01725
MS 1082	Ganesh Subramania	01725
MS 1082	William C. Sweatt	01727
MS 1082	Jason Verley	017461
MS 9018	Central Technical Files	8944 (electronic copy)
MS 0899	Technical library	4536 (electronic copy)